CHEMIJA
2025. Vol. 36. No. 1. P. 1–7

ISSN 0235-7216 eISSN 2424-4538
DOI: https://doi.org/10.6001/chemija.2025.36.1.1

Functionalisation of silver nanoparticles with 4-mercaptophenylacetic acid for iron ions detection using surface-enhanced Raman spectroscopy

Tatjana Charkova[1*],

Kristina Bolgova[2]

[1] *Department of Organic Chemistry, Center for Physical Sciences and Technology, 3 Saulėtekio Avenue, 10257 Vilnius, Lithuania*

[2] *Faculty of Chemistry and Geosciences, Vilnius University, 24 Naugarduko Street, 03225 Vilnius, Lithuania*

The detailed synthesis of silver nanoparticles (30 ± 5 nm) functionalised with 4-mercaptophenylacetic acid and their interaction with iron ions are presented. The study shows the morphological changes of the nanostructures due to the interaction with iron ions, leading to aggregation. The formation of bulky complexes is proved by UV–Vis, HR-TEM and SEM data. The complexes increase the SERS sensitivity of 4-mercaptophenylacetic acid, expanding wider analytical applications.

Keywords: silver nanoparticles, 4-mercaptophenylacetic acid, iron ions, surface-enhanced Raman spectroscopy

INTRODUCTION

Iron is necessary for many biochemical processes, such as oxygen transport to body organs, energy production, enzymatic reactions, synthesis of hormones, etc. Both iron deficiency and iron overload are associated with pathological health conditions. Iron deficiency causes weakened immunity, digestive and cognitive problems, anemia, and other diseases. On the other hand, increased iron accumulation creates toxic reactive oxygen species that can damage the heart, liver, pancreas, and other organs [1–3].

The release of iron minerals from underground mines and the corrosion of remaining constructions are the main causes of iron pollution in the environment [4]. Water, soil, plants, vegetables, etc. contaminated with iron and other heavy metals have a strong impact on nutrient quality and human health [5, 6]. Therefore, there is a growing need to develop new metal detection methodologies.

Metal ions can be effectively detected using a variety of equipment and techniques, such as optical [7], electrochemical [8] and spectroscopic methods [9]. Nanomaterial sensors are a powerful complement to the aforementioned analytical methods, providing selectivity, an increased sensitivity and a rapid monitoring without an extensive sample preparation [10–12]. Surface-enhanced Raman spectroscopy (SERS) is a simple, promising, non-invasive spectroscopic technique successfully used for the detection of heavy metals in water and food [13, 14]. Nanoactive SERS substrates are widely used for the sensitive detection of various chemical and biological analytes [15, 16]. The specific detection method using SERS is based on the aggregation of nanostructures in the presence of certain cations [17]. Plasmonic nanoparticles are functionalised with a particular analyte that reacts with cations to form aggregated complexes. The formation of such aggregates brings the nanoparticles closer together, resulting in a significant amplification of the Raman signal.

* Corresponding author. Email: tatjana.charkova@ftmc.lt

Silver nanoparticles have unique optical properties that allow them to be used in a wide wavelength range (400–1000 nm) for monitoring the intense Raman spectra of different analytes [18]. In this report, synthesised silver nanoparticles (30 ± 5 nm) were applied for detection studies. Iron ions (Fe(II) and Fe(III)) were chosen as detection cations and 4-mercaptophenylacetic acid (MPAA) as the analyte for nanoparticle functionalisation. Consequently, the prototype sensor demonstrated its suitability for detecting Fe(II) (10^{-4}–10^{-10} M) and was useless for Fe(III) ions.

EXPERIMENTAL

Materials

Silver nitrate ($AgNO_3$, 99%), trisodium citrate dihydrate (Na_3Cit, $HOC(COONa)(CH_2COONa)_2{\cdot}2H_2O$, 99%) and mili-Q water (18.2 MΩ·cm) were used for nanoparticle synthesis. 4-Mercaptophenylacetic acid (MPAA, 99%) in ethanol (C_2H_5OH, 99.8%) was chosen for nanoparticle functionalisation. Iron (II) chloride tetrahydrate ($FeCl_2{\cdot}4H_2O$, 98%) and iron (III) chloride hexahydrate ($FeCl_3{\cdot}6H_2O$, 97%) were used to prepare solutions for the detection of iron ions. All materials (Merck) were applied in all experiments without further purification.

Synthesis of nanoparticles (Ag NPs)

Na_3Cit (1%, 1 mL) was added to a boiling $AgNO_3$ (1 mM, 50 mL) solution. The reaction mixture was refluxed for 40 min, then cooled at room temperature (30 min) and in a cold water bath (30 min). The prepared suspension of yellow-greenish silver nanoparticles (Ag NPs) was stored at 5–10°C before use for further experiments.

Functionalisation of nanoparticles (Ag–MPAA NPs)

MPAA (2 mM in ethanol, 7 μL) was added to an Ag NPs suspension (5 mL) and stored at 5–10°C for 24 h. The next day functionalised silver nanoparticles (Ag–MPAA NPs) were centrifuged (20 min, 3500 rpm) and used for the binding of iron ions.

Binding of iron ions into complex (Ag–MPAA–Fe)

The centrifuged Ag–MPAA NPs (0.1 mL) were mixed with water (0.9 mL), iron ions (10^{-10}–10^{-4} M, 1 mL) and left at 5–10°C for 24 h. The next day functionalised silver nanoparticles bonded with iron ions (Ag–MPAA–Fe) were centrifuged (10 min, 3500 rpm) and used for the detection of iron ions by SERS.

EQUIPMENT AND METHODS

The synthesis mixture was refluxed using a silicone oil bath and an IKA RCT Basic magnetic stirrer. The synthesised nanoparticles were centrifuged in an Eppendorf Centrifuge 5420.

Samples for UV–Vis analysis were prepared in mili-Q water (ratio 1:100), and spectra were recorded on a Peak instruments C-7200S UV–Vis spectrophotometer.

Particle morphology analysis was performed using a Tecnai F20 X-TWIN high-resolution transmission electron microscope (HR-TEM) and a Hitachi Tabletop TM4000Plus scanning electron microscope (SEM). Confocal images were taken using an inVia Raman spectrometer (Renishaw).

SERS data were collected on a RamanFlex 400 spectrometer using a 785 nm diode laser (50 mW, 100 s). Samples for SERS were dropped (5 μL) onto a steel substrate, and spectra were recorded from the centres of the drops.

RESULTS AND DISCUSSION

Due to the affinity of carboxylic groups for cations, silver nanoparticles functionalised with organic acids, for example, lipoic acid [19], ferulic acid [20] and mercaptobenzoic acid [21], are suitable for the detection of various heavy metals. In this work, the functionalised with 4-mercaptophenylacetic acid (MPAA) silver nanoparticles (Ag–MPAA NPs) were selected for iron ion binding experiments using SERS. The thiol group of the MPAA molecule can bind to the Ag nanoparticles, free carboxylic groups can form bridges with iron ions, and the benzene ring is active in Raman spectra (Fig. 1).

Silver nanoparticles (Ag NPs) of various sizes and shapes can be produced by physical, biological and chemical approaches [22, 23]. Spherical nanoparticles are synthesised by one of the simplest methods of chemical reduction. In this work, Ag NPs were synthesised by chemical reduction in a solution using silver nitrate as a precursor, sodium citrate as a reducer and water as a solvent.

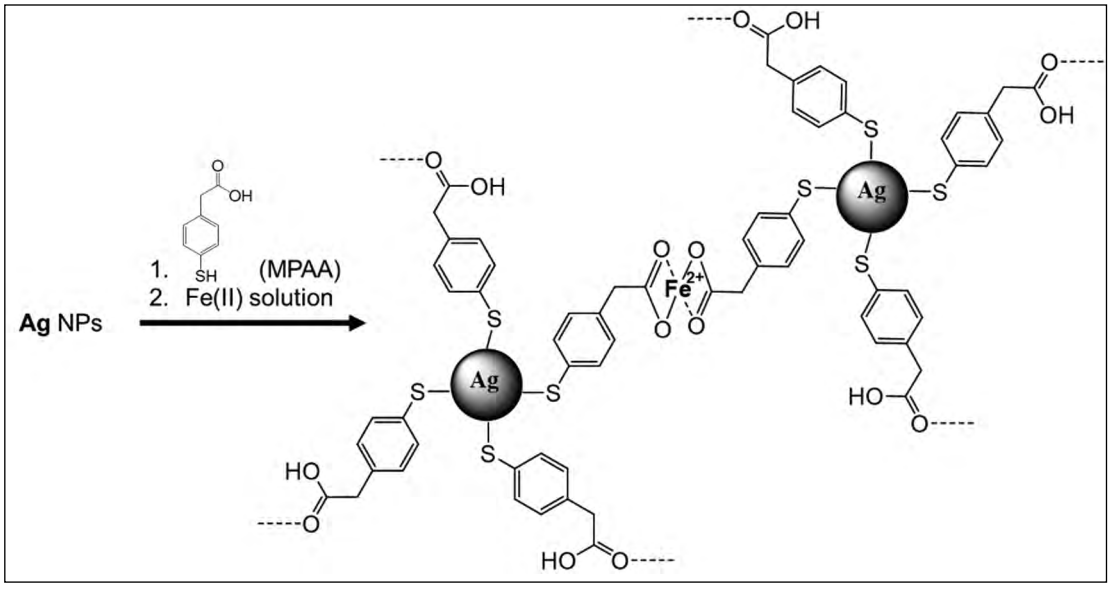

Fig. 1. Schematic illustration of Ag nanoparticles functionalisation and iron ion binding

Conventional (20–100 nm) citrate-coated silver nanospheres have absorption in the 400–500 nm UV spectral range [24]. The produced Ag NPs showed UV absorption at 402 nm (Fig. 2). Next, a previously described methodology [21] was adapted for the functionalisation of Ag NPs using an MPAA analyte. The absorption maximum shifted from 402 to 405 nm after nanoparticle functionalisation.

The HR-TEM analysis confirmed the spherical shape and small size (30 ± 5 nm) of the synthesised Ag nanoparticles (Fig. 3a). Next, the functionalised Ag-MPAA nanoparticles were mixed with (10^{-2} M) aqueous solutions of Fe(II) and Fe(III) ions, which caused a rapid aggregation and discoloration of the mixtures (Fig. 2). The yellow-green suspension of Ag–MPAA nanoparticles faded in the presence of Fe(III) ions and darkened in the presence of Fe(II) ions. A noticeable change was also observed in the UV–Vis spectra (Fig. 2). The Ag–MPAA particles dissolved in the Fe(III) solution, no absorption

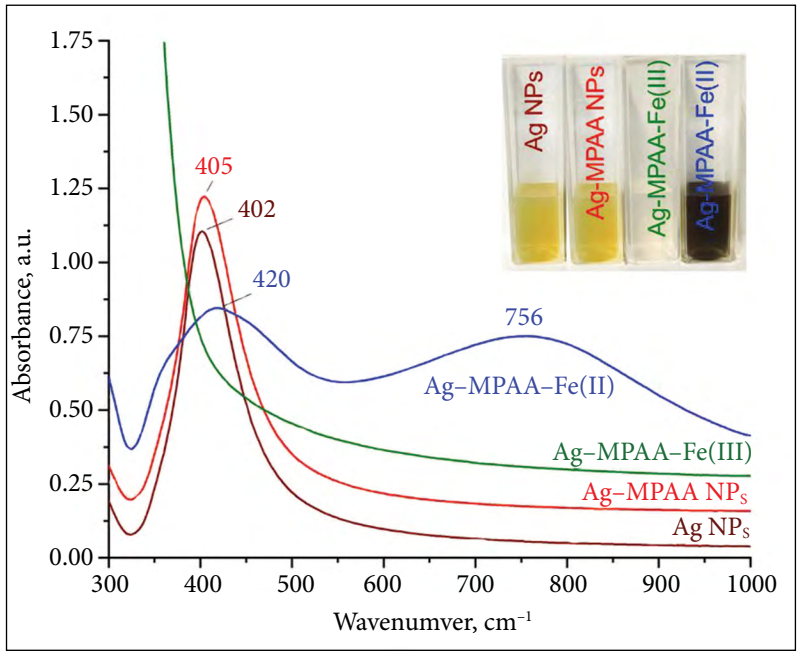

Fig. 2. Photos and UV–Vis spectra of Ag nanoparticles, functionalised Ag-MPAA nanoparticles, Ag–MPAA–Fe(III) and Ag–MPAA–Fe(II) complex

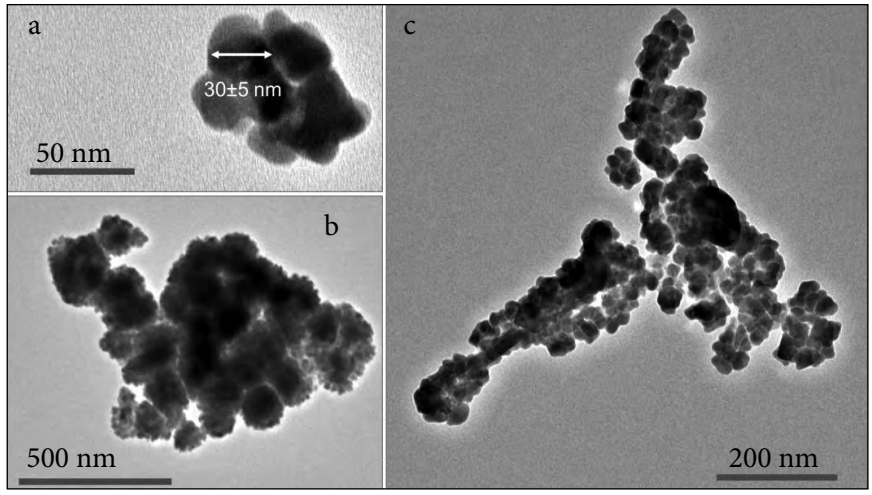

Fig. 3. HR-TEM images of Ag nanoparticles (a), functionalised Ag–MPAA nanoparticles (b) and Ag–MPAA–Fe(II) complex (c)

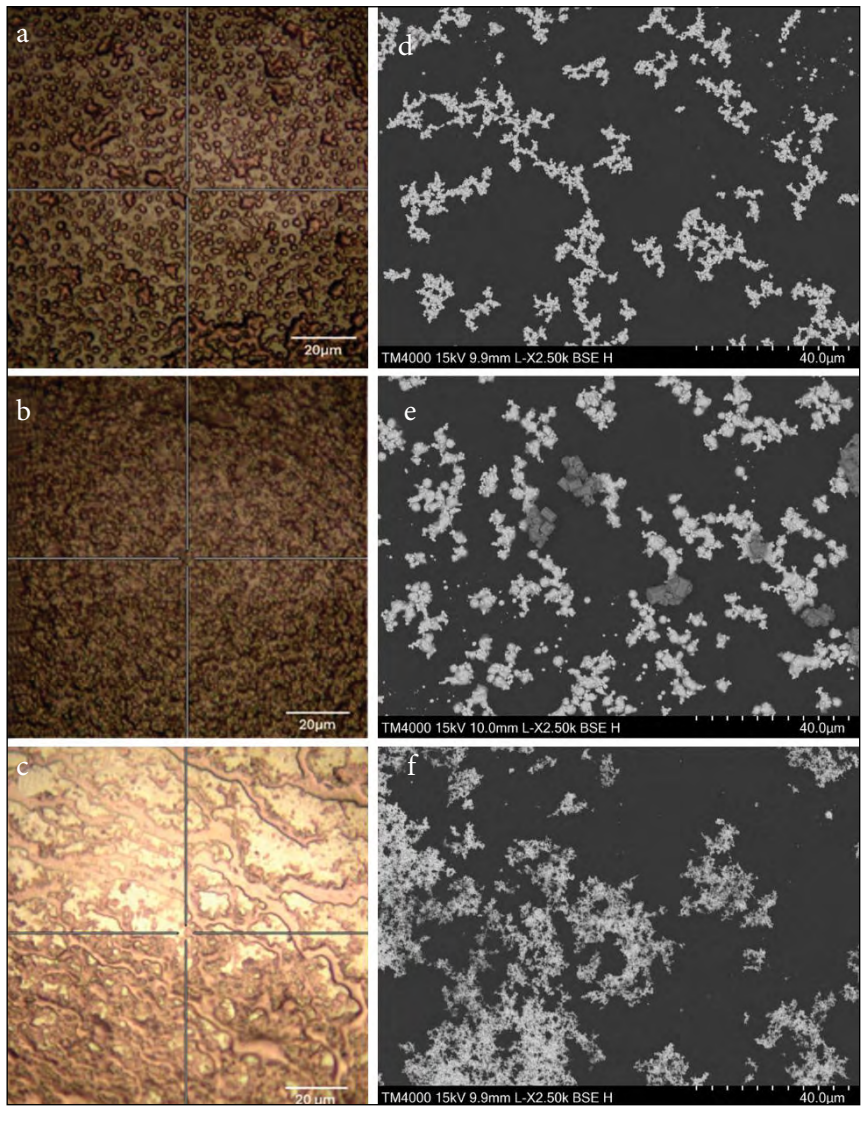

Fig. 4. Confocal Raman spectroscope images of Ag nanoparticles (a), Ag–MPAA nanoparticles (b) and Ag–MPAA–Fe(II) complex (c). SEM images of Ag nanoparticles (d), Ag–MPAA nanoparticles (e) and Ag–MPAA–Fe(II) complex (f)

peak of nanoparticles was observed in the UV spectrum. In the case of Fe(II), a broadening peak at 420 nm was detected, which indicates the formation of nanostructures of different sizes [25]. UV absorption above 850 nm has been previously reported to be associated with Ag-aggregated complexes of heavy metals [21]. The absorption of Ag–MPAA–Fe(II) complex was detected at 756 nm (Fig. 2). The HR-TEM analysis also confirmed that the functionalised Ag–MPAA nanoparticles formed aggregates in the presence of Fe(II) ions (Fig. 3b, c).

The Ag–MPAA–Fe complex formation requires free carboxylic groups, so the SH groups of the analyte are oriented to Ag, and the free COOH to the solution (Fig. 1). Otherwise oriented MPAA molecules would not form the aggregated complex. The formation of the Ag–MPAA–Fe(II) complex was proved by several methods. First of all, this was noticeable visually – in the presence of Fe(II) ions, a dark suspension immediately appears (Fig. 2). The UV–Vis spectrum also characterised the structural changes of the functionalised Ag–MPAA nanoparticles – nanoparticles aggregated and a new absorption maximum (>750 nm) occurred (Fig.2). The HR-TEM analysis confirmed the formation of bulky (>500 nm) aggregates (Fig. 3c). The aggregation process was also noticeable on the confocal Raman spectroscope images (Fig. 4a–c). The SEM analysis was performed in parallel and also allowed the observation of aggregation (Fig. 4d–f).

The nanoparticles functionalised with COOH groups get closer in the presence of cations because coordination bonding connects several carboxylic residues adsorbed on different nanoparticles (Fig. 1). The formation of such regions leads to hot spots and significantly increases the SERS enhancement [26]. This allows the detection of cations by SERS.

The MPAA molecule adsorbs on the surface of Ag nanoparticles through Ag–S bonds. To demonstrate this, Ag nanoparticles were mixed with 10^{-2} M MPAA analyte and the Raman spectrum was recorded by observing Ag–S at approximately 240 cm^{-1} (Fig. 5c). The Raman spectrum of Ag nanoparticles was also recorded and the main impurities (933, 1021, 1392 cm^{-1}) were indicated (Fig. 5a). The other vibrational bands of MPAA were successfully detected (Fig. 5c). All assignments were based on the previously reported spectral analyses of mercaptobenzyl and mercaptophenyl derivatives [27–30] and are presented in the Table.

The SERS spectrum of functionalised Ag-MPAA nanoparticles recorded from a drop was not informative – no vibrational bands of MPAA molecule were observed (Fig. 6a). A small diameter

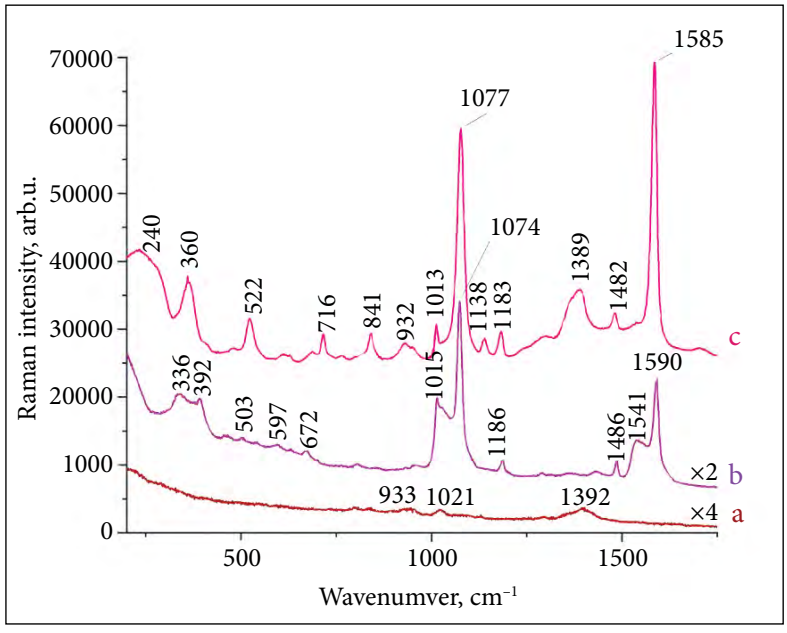

Fig. 5. Raman spectra (recorded on steel): Ag nanoparticles (a), Ag–MPAA–Fe(II) complex (b), the mixture of Ag nanoparticles and (10^{-2} M) MPAA analyte (c)

Table. **Main spectral assignments of MPAA**

Wavenumber, cm^{-1}	Assignments
240	Ag–S stretching
360	CCC out-of-plane bending
522	ring out-of-plane bending
716	CCC out-of-plane bending
841	COO- bending
1013	ring breathing
1077	ring breathing, C–S stretching, C–H in-plane bending
1138	C–H bending
1183	C–H bending
1389	COO- stretching
1482	ring bending
1585	ring C–C stretching, C–H in-plane bending

of nanoparticles (about 35 nm) does not cause a strong Raman enhancement effect from a nearby environment, because of a low concentration of the adsorbed MPAA (see Experimental). However, the size of nanoparticles was suitable for the formation of aggregated Ag–MPAA–Fe(II) complex, which caused a noticeable Raman enhancement (Fig. 5b). The vibrational modes at about 330–400 and 500–700 cm^{-1} appeared in the spectrum, which probably can be attributed to Fe–O stretching vibrations [31, 32]. In addition, ring deformation (522 and 716 cm^{-1}) and COO^- vibration modes (841 and 1389 cm^{-1}) disappeared. The benzene ring vibration changes immediately, because COO^- groups bind Fe(II). The most intense peaks associated with the ring showed a significant doubling at 1015, 1074 cm^{-1} and 1541, 1590 cm^{-1}. These apparent spectral changes were important in the detection of Fe(II) ions by SERS.

To demonstrate the sensitivity of the method, the 10^{-10}–10^{-4} M Fe(II) solutions were tested. All recorded SERS spectra were informative (Fig. 6a) – the main MPAA bands that were observed coincide with those previously discussed. The dominant vibrational mode of MPAA (1074 cm^{-1}) was chosen to show the dependence of Raman intensity on the Fe(II) concentration (Fig. 6b). An increase in the Fe(II) concentration results in more hot spots, which increase the intensity of the Raman signal.

CONCLUSIONS

Silver nanoparticles (30 ± 5 nm) were synthesised and functionalised with 4-mercaptophenylacetic acid (MPAA). The functionalised nanoparticles (Ag–MPAA) were successfully applied for binding Fe(II) ions from aqueous solutions (10^{-10}–10^{-4} M). The nanoparticle aggregation into a bulky complex in the presence of Fe(II) ions was proved by UV–Vis, HR-TEM, SEM and SERS techniques. However, the sensor prototype was not suitable for the detection of Fe(III) ions.

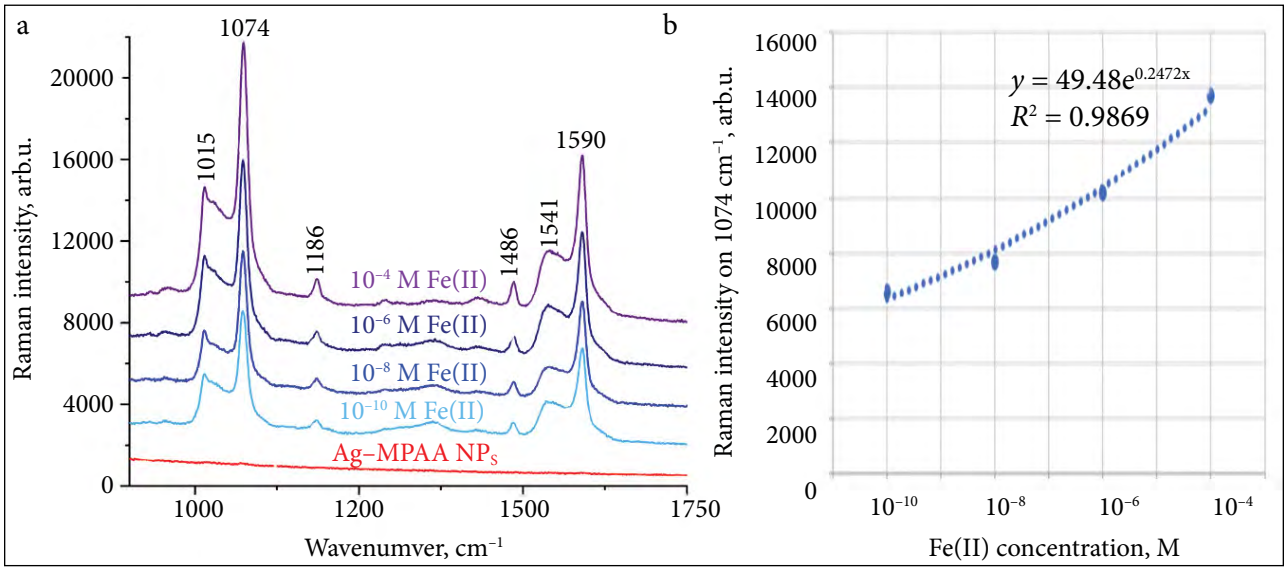

Fig. 6. Raman spectra (recorded on steel) of the functionalised Ag–MPAA nanoparticles and the Ag–MPAA–Fe(II) complex formed with 10^{-10}–10^{-4} M Fe(II) (a). Dependence of 1074 cm^{-1} peak Raman intensity on Fe(II) concentration (b)

ACKNOWLEDGEMENTS

The project has received funding from the European Social Fund (Project No. P-SV-24-942) under a Grant Agreement with the Research Council of Lithuania (LMTLT).

The authors thank the colleagues for the opportunity to use the equipment, Ilja Ignatjev for the Raman confocal images, Audrius Drabavičius for the HR-TEM and Karina Vjūnova for the SEM recordings.

Received 8 January 2025
Accepted 22 January 2025

References

1. P. T. Lieu, M. Heiskala, P. A. Peterson, Y. Yang, *Mol. Asp. Med.*, **22**, 1 (2001).
2. F. Oliveira, S. Rocha, R. Fernandes, *J. Clin. Lab. Anal.*, **28**, 210 (2014).
3. A. Lal, *Indian J. Pediatr.*, **87**, 58 (2020).
4. L. Zhou, J. Y. Zhang, X. Q. Zhu, D. M. Xu, S. S. Zheng, *J. Clean. Prod.*, **471**, 143358 (2024).
5. J. Manzoor, M. Sharma, K. A. Wani, *J. Plant. Nutr.*, **41**, 1744 (2018).
6. A. Zwolak, M. Sarzyńska, E. Szpyrka, K. Stawarczyk, *Water Air Soil Pollut.*, **230**, 164 (2019).
7. Y.-nan Zhang, Y. Sun, L. Cai, Y. Gao, Y. Cai, *Measurement*, **158**, 107742 (2020).
8. B. K. Bansod, T. Kumar, R. Thakur, S. Rana, I. Singh, *Biosens. Bioelectron.*, **94**, 443 (2017).
9. L. A. Malik, A. Bashir, A. Qureashi, A. H. Pandith, *Environ. Chem. Lett.*, **17**, 1495 (2019).
10. S. Mao, J. Chang, G. Zhou, J. Chen, *Small*, **11**, 5336 (2015).
11. M. R. Willner, P. J. Vikesland, *J. Nanobiotechnol.*, **16**, 1 (2018).
12. H. Liaquat, M. Imran, S. Latif, N. Hussain, M. Bilal, *Environ. Res.*, **214**, 113795 (2022).
13. G. Xu, P. Song, L. Xia, *Nanophotonics*, **10**, 4419 (2021).
14. Z. Guo, P. Chen, N. Yosri, et al., *Food Rev. Int.*, **39**, 1440 (2023).
15. T. Y. Jeon, D. J. Kim, S. G. Park, S. H. Kim, D. H. Kim, *Nano Converg.*, **3**, 1 (2016).
16. P. A. Mosier-Boss, *Nanomater.*, **7**, 142 (2017).
17. R. A. Alvarez-Puebla, L. M. Liz-Marzán, *Angew. Chem. Int. Ed.*, **51**, 11214 (2012).
18. R. Pilot, R. Signorini, C. Durante, L. Orian, M. Bhamidipati, L. Fabris, *Biosensors*, **9**, 57 (2019).
19. K. Teeparuksapun, N. Prasongchan, A. Thawonsuwan, *Anal. Sci.*, **35**, 371 (2019).
20. S. Sharma, A. Jaiswal, K. N. Uttam, *Anal. Lett.*, **55**, 715 (2022).
21. E. Daublytė, A. Zdaniauskienė, M. Talaikis, T. Charkova, *J. Nanopart. Res.*, **26**, 1 (2024).
22. J. Natsuki, *Int. J. Mater. Sci. Appl.*, **4**, 325 (2015).
23. O. Pryshchepa, P. Pomastowski, B. Buszewski, *Adv. Colloid Interface Sci.*, **284**, 102246 (2020).
24. D. Paramelle, A. Sadovoy, S. Gorelik, P. Free, J. Hobley, D. G. Fernig, *Analyst*, **139**, 4855 (2014).
25. R. Desai, V. Mankad, S. K. Gupta, P. K. Jha, *Nanosci. Nanotechnol. Lett.*, **4**, 30 (2012).
26. A. Rai, S. Bhaskar, K. M. Ganesh, S. S. Ramamurthy, *ACS Appl. Nano Mater.*, **5**, 12245 (2022).
27. H. Su, Y. Wang, Z. Yu, et al., *Spectrochim. Acta A Mol. Biomol. Spectrosc.*, **185**, 336 (2017).
28. M. J. Trujillo, J. P. Camden, *ACS Omega*, **3**, 6660 (2018).
29. C. K. A. Nyamekye, S. C. Weibel, E. A. Smith, *J. Raman Spectrosc.*, **52**, 1246 (2021).
30. E. Daublytė, A. Zdaniauskienė, M. Talaikis, A. Drabavičius, T. Charkova, *New J. Chem.*, **45**, 10952 (2021).
31. N. Boucherit, A. Hugot-Le Goff, S. Joiret, *Corros. Sci.*, **32**, 497 (1991).
32. D. L. A. de Faria, S. V. Silva, M. T. de Oliveira, *J. Raman Spectrosc.*, **28**, 873 (1997).

Tatjana Charkova, Kristina Bolgova

SIDABRO NANODALELIŲ FUNKCIONALIZAVIMAS 4-MERKAPTOFENILACTO RŪGŠTIMI GELEŽIES JONAMS APTIKTI, NAUDOJANT PAVIRŠIAUS SUSTIPRINTĄ RAMANO SPEKTROSKOPIJĄ

S a n t r a u k a

Cheminės redukcijos metodu susintetintos sidabro nanosferos (30 ± 5 nm) buvo funkcionalizuotos 4-merkaptofenilacto rūgštimi. Funkcionalizuotos dalelės parodė gimiringumą Fe(II) katijonams, surišant juos į kompleksus. Morfologiniai nanostruktūrų pokyčiai, agregacija ir kompleksų susidarymas buvo patvirtinti UV-Vis, HR-TEM ir SEM duomenimis. Agreguoti kompleksai taip pat padidina 4-merkaptofenilacto rūgšties Ramano signalų jautrumą, išplečiant paviršiaus sustiprintos Ramano spektroskopijos metodo pritaikomumą geležies jonams aptikti.

Projektas buvo bendrai finansuotas iš Europos socialinio fondo lėšų (projekto Nr. P-SV-24-942) pagal dotacijos sutartį su Lietuvos mokslo taryba (LMT LT).